Experimental study of isomeric intruder 1/2^{+} states in ^{197,203}At

K. Auranen, J. Uusitalo, S. Juutinen, H. Badran, F. Defranchi Bisso, D. Cox, T. Grahn, P. T. Greenlees, A. Herzáň, U. Jakobsson, R. Julin, J. Konki, M. Leino, A. Lightfoot, M. Mallaburn, O. Neuvonen, J. Pakarinen, P. Papadakis, J. Partanen, P. Rahkila, M. Sandzelius, J. Sarén, C. Scholey, J. Sorri, and S. Stolze

Phys. Rev. C **95**, 044311 — Published 10 April 2017

DOI: 10.1103/PhysRevC.95.044311

Experimental study of isomeric intruder $^1/_2^+$ states in ^{197,203}At

K. Auranen,[1,2,*] J. Uusitalo,[1] S. Juutinen,[1] H. Badran,[1] F. Defranchi Bisso,[1] D. Cox,[1] T. Grahn,[1] P.T. Greenlees,[1] A. Herzáň,[1,†] U. Jakobsson,[3,‡] R. Julin,[1] J. Konki,[1] M. Leino,[1] A. Lightfoot,[1] M. Mallaburn,[4] O. Neuvonen,[1] J. Pakarinen,[1] P. Papadakis,[1] J. Partanen,[1] P. Rahkila,[1] M. Sandzelius,[1] J. Sarén,[1] C. Scholey,[1] J. Sorri,[1] and S. Stolze[1]

[1] *University of Jyvaskyla, Department of Physics, P.O. Box 35, FI-40014 University of Jyvaskyla, Finland*
[2] *Argonne National Laboratory, 9700 South Cass ave, Lemont, Illinois 60439, USA*
[3] *Department of Physics, Royal Institute of Technology, SE-10691 Stockholm, Sweden*
[4] *University of Manchester, Manchester M13 9PL, United Kingdom*

(Dated: March 10, 2017)

A newly observed isomeric intruder $^1/_2^+$ state [$T_{1/2}$ = 3.5(6) ms] is identified in ^{203}At using a gas-filled recoil separator and fusion-evaporation reactions. The isomer is depopulated through a cascade of E3 and mixed M1/E2 transitions to the $^9/_2^-$ ground state, and it is suggested to originate from the $\pi(s_{1/2})^{-1}$ configuration. In addition, the structures above the $^1/_2^+$ state in ^{203}At and ^{197}At are studied using in-beam γ-ray spectroscopy, recoil-decay tagging and recoil-isomer decay tagging methods. The $^1/_2^+$ state is fed from $^3/_2^+$ and $^5/_2^+$ states, and the origin of these states are discussed.

I. INTRODUCTION

When a proton from the $s_{1/2}$ orbital is excited across the Z = 82 magic shell gap, an intruder $^1/_2^+$ state is formed. This is energetically reasonable if the nucleus is considered to be slightly oblate deformed, in which case the $\frac{1}{2}$[400] Nilsson orbital approaches the Fermi surface rapidly. Such a state is usually an isomeric state in odd-mass neutron deficient nuclei heavier than lead, but in some cases it becomes the ground state. In bismuth nuclei this state is well known. The level energy is pushed down as the neutron number decreases, and it becomes the ground state in ^{185}Bi ([1], and references therein).

In odd-mass astatine nuclei this state is known in isotopes $^{191-201}$At [2–5]. It was first observed in ^{197}At, where it is known to be an α-decaying isomeric state, which lies 52 keV above the ground state. In ^{195}At it becomes the ground state. The corresponding state is also known in a few francium nuclei. It is an isomeric excited state in odd-mass isotopes $^{201-205}$Fr [6–8], and in ^{199}Fr it may become the ground state [6, 9, 10].

The level patterns above these states are of interest. In bismuth nuclei ^{191,193}Bi a rotational like bands are observed to feed the isomeric state [11, 12]. In heavier isotopes ^{203,205,207}Bi the isomer is fed from nearly spherical $^3/_2^+$ and $^5/_2^+$ states originating from the intruder configurations of $\pi(d_{3/2})^{-1}$ and $\pi(d_{5/2})^{-1}$, respectively [13]. Recently it was also observed that a superdeformed band is partially depopulated to the $^1/_2^+$ state in ^{193}Bi [12]. Also a couple of candidates for the feeding states in ^{205}Fr are suggested [8]. Our recent study [5] presented the level structures above the $^1/_2^+$ states in ^{199,201}At. Similarly to heavier bismuth isotopes, the two lowest levels above the $^1/_2^+$ state were suggested to have a spin and parity of $^3/_2^+$ and $^5/_2^+$, and those were suggested to originate from the $\pi(d_{3/2})^{-1}$ and $\pi(d_{5/2})^{-1}$ configurations, respectively.

In this publication we present the feeding and depopulation of the isomeric intruder $^1/_2^+$ state in ^{203}At. This is the first observation of this state in ^{203}At. In addition we propose a preliminary level pattern above the $^1/_2^+$ state in ^{197}At. Also a discussion about the origin of the levels above the isomeric $^1/_2^+$ state is presented.

II. EXPERIMENTAL SETUP

The nuclei of interest were produced using the ^{159}Tb(^{48}Ca,4n)^{203}At and ^{165}Ho(^{36}Ar,4n)^{197}At fusion-evaporation reactions. The α-particle energy spectra shown in Fig. 1 can be used to estimate the relative production yields. The self-supporting targets had thicknesses of 360 and 350 μg/cm^2, respectively. In both parts of the experiment a carbon reset foil (79 μg/cm^2) was stacked behind the target. The beams were produced with the K-130 cyclotron in the Accelerator Laboratory at the Department of Physics at the University of Jyväskylä. The beam energies of 198 MeV and 173 MeV, typical beam intensities of 10 pnA and 25 pnA, and irradiation times of 70 h and 180 h were used to produce ^{203}At and ^{197}At, respectively. In Fig. 1(a) one can observe some contaminant α-activities. The energies of these are close to the α-particle energies of ^{202}Rn, ^{203m}Rn, ^{199}At and ^{200m}At, which would have been produced in pxn and αxn-evaporation channels if there was a ^{48}Ti contaminant in the ^{48}Ca beam.

The fusion-evaporation residues (later recoils) were separated from the primary beam and other unwanted particles by using the He-filled recoil separator RITU [14, 15]. A flight time through RITU was in the order of 0.6 and 0.8 μs for ^{203}At and ^{197}At recoils, respectively. A transmission detector, in this case a multiwire pro-

* kauranen@anl.gov
† Present address: Oliver Lodge Laboratory, University of Liverpool, Liverpool L69 7ZE, United Kingdom
‡ Present address: Laboratory of Radiochemistry, Department of Chemistry, P.O. Box 55, FI-00014 University of Helsinki, Finland

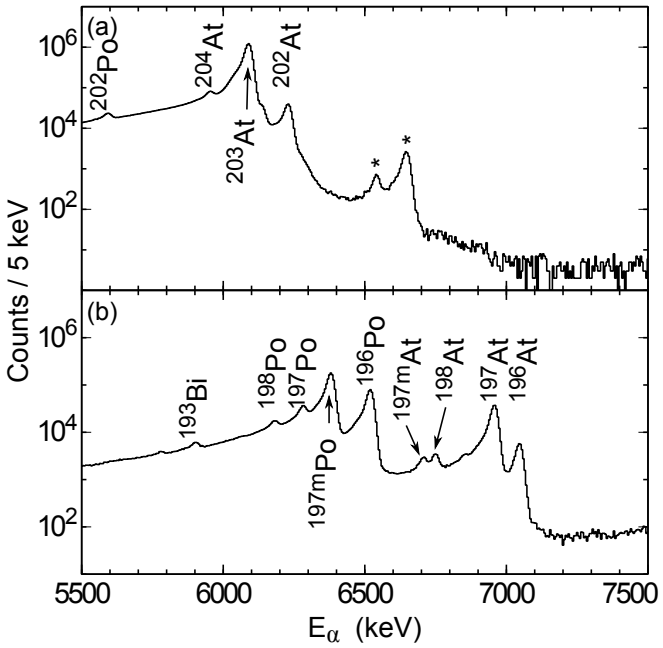

FIG. 1. MWPC vetoed α-particle energy spectrum observed in the DSSD obtained with (a) ^{48}Ca(198 MeV) + ^{159}Tb and (b) ^{36}Ar(173 MeV) + ^{165}Ho reactions. Activities marked with an asterisk most likely originate from a contaminant ^{48}Ti beam, see text for details.

portional counter (MWPC), was placed upstream from RITU's focal plane. At the focal plane the recoils were studied using the GREAT spectrometer [16]. The recoils were implanted into a 300-μm-thick double-sided silicon strip detector (DSSD), which was surrounded by a box array of silicon detectors consisting of 28 PIN diodes. Both of these silicon detector setups were adjusted to detect α particles and conversion electrons. At the focal plane delayed γ rays were detected with three clover type germanium detectors and one planar type germanium detector. The clover detectors were positioned in close geometry around the DSSD vacuum chamber. The planar detector was placed immediately behind the DSSD inside the GREAT vacuum chamber, and it was efficient for detecting x-rays and low-energy γ rays.

The JUROGAM II array, consisting of 24 clover [17] and altogether 15 Phase1 [18] and GASP [19] type Compton suppressed germanium detectors, was placed around the target position to observe prompt γ rays. The angular distributions of prompt γ rays observed in this experiment showed some irregularities when plotted against $\cos^2(\theta)$. Here θ denotes the angle between beam axis and a detector. Because of this, it was not possible to extract the exact value of the angular distribution parameter A_2 [20]. However, a clear descending (A_2<0) or ascending (A_2>0) trend was observed for transitions which were previously [21] assigned as a stretched dipole or stretched quadrupole transitions, respectively. This issue might arise due to a misplaced target and/or calibration source. An add-back method was implemented to the analysis of γ-ray data from all clover-type detectors.

A triggerless total data readout method (TDR) [22] was used to collect data from all ADC channels independently. Data analysis of prompt γ rays was based on the recoil-decay tagging (RDT) and the recoil-isomer decay tagging methods. All events were timestamped with a 100 MHz clock. The data analysis were performed with GRAIN [23] software package.

III. RESULTS

A. $^1/_2^+$ state in ^{203}At.

The search of the isomeric, intruder $^1/_2^+$ state in ^{203}At was based on a search of recoil implantation followed by a conversion electron in the same pixel of the DSSD (later R-e$^-$). The allowed correlation time between these two events was set to be 0.1-13 ms. The lower limit is required in order to suppress the events related to a shorter living high-spin isomeric state in ^{203}At [24]. The maximum correlation time of 13 ms is roughly 4 times the half-life of the $^1/_2^+$ isomer. The deduction of the half-life will be explained later in this section. The identification of a recoil was based on the time-of-flight from the MWPC to the DSSD and to the energy loss of the recoil in the MWPC.

Fig. 2(a) presents the energy spectrum of γ rays in prompt coincidence with the R-e$^-$ chain electron. Two interesting γ-ray transitions are observed, one with an energy of 221.4(2) keV and the other with an energy of 462.0(2) keV. The third peak, with an energy of 511 keV, is the outcome of an annihilation of a positron originating from a (long-lived) β^+ activities, which are (randomly) correlated with recoil events.

In the panel (b) of Fig. 2 the energy spectrum of internal conversion electrons observed in the PIN box detector array is shown. A prompt coincidence with the R-e$^-$ chain electrons (in DSSD) is required, and the R-e$^-$ chain electron must have an energy corresponding to K or L+M+... conversion of the 221-keV transition. The two peaks in the spectrum correspond to K and L+M+... conversion of the 462 keV transition. The deduced intensity ratio of $^K/_{L+M+...} = 0.85(8)$ matches with the theoretical intensity ratio of 0.83(2) calculated for a 462-keV E3 transition [25], hence the 462-keV transition is assigned to have E3 character. Simulated efficiency information [26] was used in the deduction of the experimental $^K/_{L+M+...}$ intensity ratio. The conversion electrons from the 462-keV transition are energetic enough to punch through the DSSD, hence the thicker PINs are used in this intensity ratio analysis.

Fig. 2(c) shows the energy spectrum of R-e$^-$ chain electrons, when the electrons are observed to be in prompt coincidence with the 462-keV γ ray in the focal-plane clover array. The two peaks in the spectrum are the K and L+M+... conversions of the 221 keV transition. The intensity ratio $^K/_{L+M+...} = 1.67(10)$ was extracted,

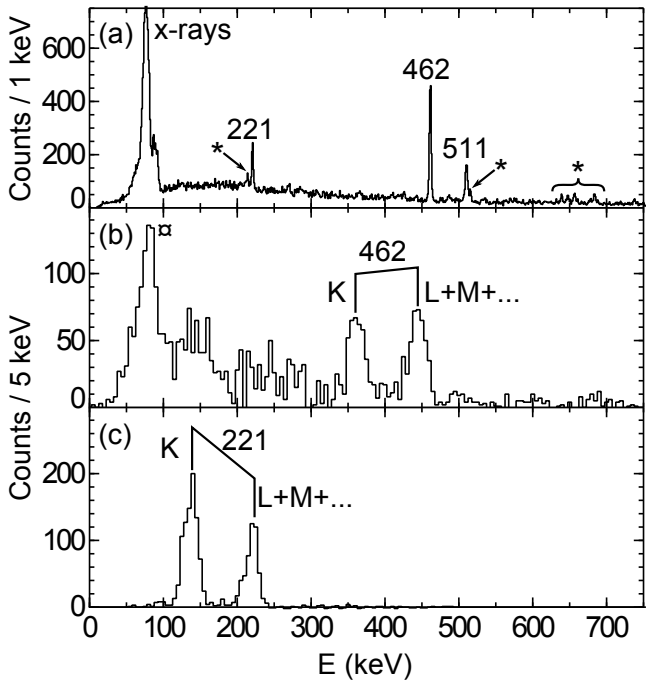

FIG. 2. (a) Energy spectrum of delayed γ rays observed in the focal-plane clover array in prompt coincidence with the R-e$^-$ chain electrons. Transitions marked with an asterisk belong to ^{203,204}At or one of their decay products, and those are not relevant for this study. (b) Energy spectrum of conversion electrons observed in the PIN diodes in coincidence with the R-e$^-$ chain electron. Electron energy of 221-K or 221-L+M+... conversion is demanded for the R-e$^-$ chain electron in DSSD. The low energy peak marked with ¤ is a spurious peak related to the structure of the PIN diodes. (c) R-e$^-$ tagged conversion electron energy spectrum observed in the DSSD. R-e$^-$ chain electron must be in prompt coincidence with the 462 keV γ ray observed in the focal-plane clover array.

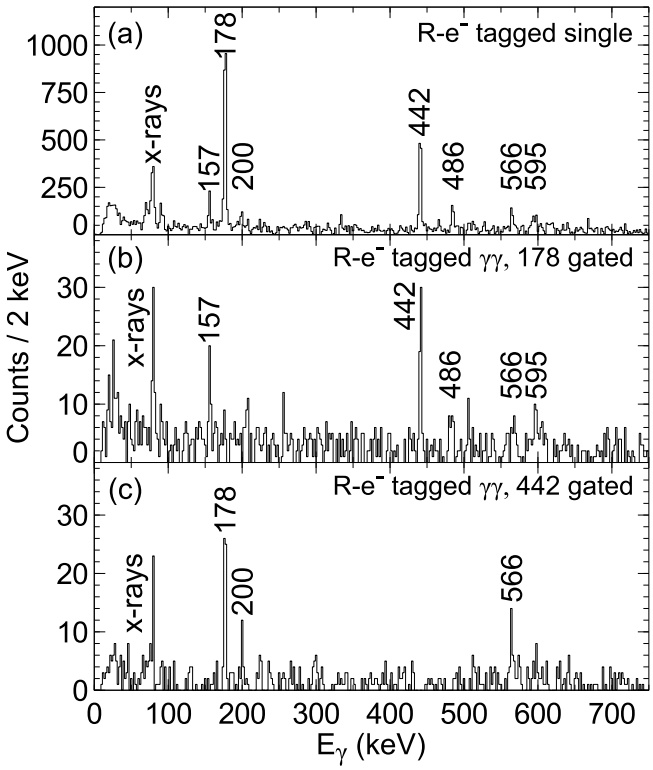

FIG. 3. (a) Energy spectrum of R-e$^-$ tagged prompt γ rays observed in JUROGAM II. Electron energy corresponding to K or $L+M+\ldots$ conversion electron energy of the 221-keV transition is demanded. Two examples of R-e$^-$ tagged $\gamma\gamma$ coincidence analysis are presented in panels (b) and (c), where the energy spectra of γ rays in coincidence with 178- or 442-keV transitions are shown, respectively.

which is between the theoretical ratios of 0.617(12) and 4.28(9) calculated [25] for pure E2 and M1 type 221-keV transitions, respectively. Moreover, the 221-keV transition is observed to be in prompt coincidence with the 462-keV transition, hence higher multipolarity assignment is unlikely. Because of these two reasons a mixed M1/E2 character is suggested for the 221-keV transition.

In Fig. 3(a) the R-e$^-$ tagged γ-ray singles energy spectrum observed in JUROGAM II is shown. Electron energies corresponding to K or $L+M+\ldots$ conversion of the 221-keV transition were required for the R-e$^-$ event chain electrons. The observed γ-ray transitions are listed in Table I. The level scheme above the $^1/_2{}^+$ isomer was built based on the $\gamma\gamma$ coincidences, γ-ray energy sums and intensity balance. Also, the angular distribution of γ rays was deduced when possible. The deduced level scheme is presented in Fig. 4. Two examples of the $\gamma\gamma$ coincidence analysis are presented in Fig. 3 panels (b) and (c). Moreover, the total transition intensity of the 442-keV and 178-keV transitions, which is extracted from the $\gamma\gamma$ spectrum gated with the 566-keV transition, must

TABLE I. Observed γ-ray transitions above the $^1/_2{}^+$ state in ^{203}At. I_γ is the relative γ-ray intensity and A_2 is the angular distribution parameter, both are deduced from R-e$^-$ tagged JUROGAM II data. Internal-conversion coefficients for the calculation of total transition intensity I_{TR} were taken from [25]. I_{TR} is normalized such that the 178-keV γ-transition has an intensity of 100.

E_γ (keV)	I_γ	I_{TR}	A_2	I_i^π	I_f^π
156.6(5)	15.7(11)	68(5), 35(3)[a]		$^5/_2{}^+$	$^3/_2{}^+$
177.9(5)	100(5)	335(14), 176(8)[a]		$^3/_2{}^+$	$^1/_2{}^+$
200.1(5)	10.8(9)	29(3)	(<0)[b]	($^9/_2{}^+$)	$^7/_2{}^+$
442.2(6)	82(4)	85(4)	>0	$^7/_2{}^+$	$^3/_2{}^+$
486.1(6)	25(2)	26(2)	>0	($^9/_2{}^+$)	$^5/_2{}^+$
566.4(9)[b]	20(2)	21(2)	>0	$^{11}/_2{}^+$	$^7/_2{}^+$
594.7(6)	16.2(13)	17(2)		($^{13}/_2{}^+$)	($^9/_2{}^+$)

[a] Transition is suggested to have a mixed M1/E2 character. The two given intensity readings stand for pure M1 and E2 transition, respectively.

[b] Deduced from the R-e$^-$ tagged 442-keV gated $\gamma\gamma$ coincidence data

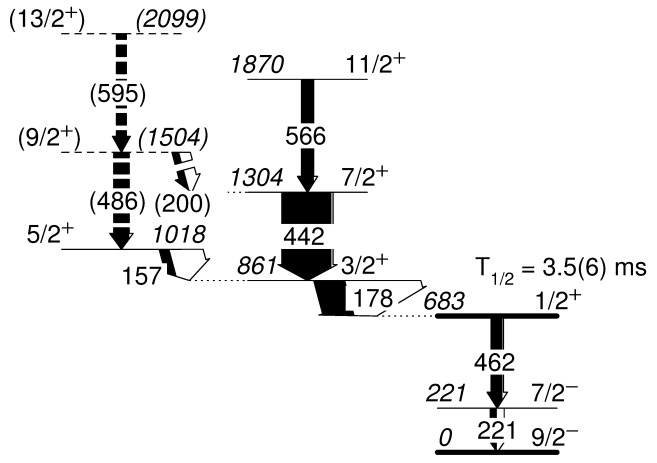

FIG. 4. Level scheme of the $^1/_2^+$ structure in ^{203}At. The intensities of the transitions below the $^1/_2^+$ state and the 178-keV transition are not to scale.

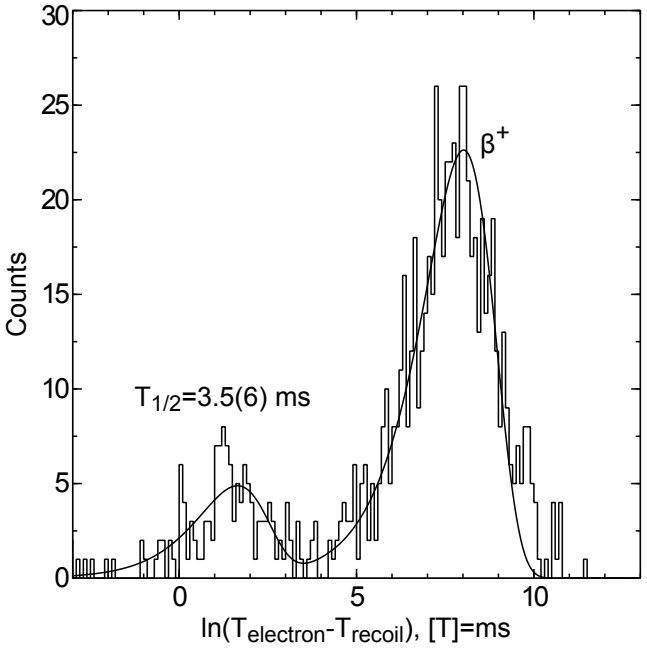

FIG. 5. Natural logarithm of the time difference between the recoil implantation and the subsequent electron in the same pixel of the DSSD. The electron must be in prompt coincidence with the 462-keV γ ray observed in the focal-plane clover array, and the recoil must be correlated with the 178-keV or 442-keV prompt γ ray in JUROGAM II array. A logarithmic time-scale method [27] yields a half-life of 3.5(6) ms. The longer living component is a result of random coincidences of β^+ particles and γ rays.

be identical. As the 442-keV transition is suggested to be of type $E2$ based on the angular distribution of γ rays, the type of the 178-keV transition can be deduced. This analysis excludes pure $E1$ and $E2$ characters, and suggests either pure $M1$ or mixed M1/E2 character for the 178-keV transition. The angular distribution of the 178-keV γ rays does not reflect the angular distribution of a pure stretched dipole, hence a mixed M1/E2 character is suggested. This is also the assignment of both analogous transitions in neighboring ^{199,201}At nuclei [5], and the observed x-ray yields in Fig. 3 support this picture. Also, the angular distribution of the 157-keV γ rays reflect neither the angular distribution of a stretched dipole nor quadrupole, hence also this transition is suggested to have a mixed M1/E2 character.

The time distribution between the recoil implantation and the subsequent electron is presented in Fig. 5. As the $^1/_2^+$ state is non-yrast, it is weakly populated in fusion-evaporation reactions, hence selective tagging methods are required in order to extract the half-life of the state. The R-e$^-$ chain electron must be in coincidence with the 462-keV γ ray observed in any of the focal plane clover detectors. In addition, the recoil must be correlated with the 178-keV or 442-keV prompt γ ray observed in JUROGAM II array. Once these two conditions are introduced the $^1/_2^+$ state related events are separated from the random background. The background is mainly β^+ particles in coincidence with (Compton scattered) γ rays. A half-life of 3.5(6) ms was extracted by using a logarithmic time-scale method [27].

B. Level pattern above the $^1/_2^+$ state in ^{197}At.

In ^{197}At the $^1/_2^+$ state is known to lie at the excitation energy of 52(10) keV, and it decays by α-particle emission ($E_\alpha = 6707(5)$ keV, $T_{1/2} = 2.0(2)$ s [30]). These α-decay properties partially overlap with the α-decay properties of ^{198}At ($E_\alpha = 6748(6)$ keV, $T_{1/2} = 3.8(4)$ s [6]) and ^{195m}Po ($E_\alpha = 6699(5)$ keV, $T_{1/2} = 1.92(2)$ s [31]). In this study some amounts of these nuclei were produced as side products.

Because of this, the recoil - ^{197}At($^1/_2^+$) α-decay tagging (later R-α) is not a sufficient method to reliably recognize the γ-ray transitions feeding the $^1/_2^+$ state in ^{197}At. Therefore recoil - ^{197}At($^1/_2^+$) α-decay - ^{193}Bi($^1/_2^+$) α-decay tagging (later R-α-α) was introduced. The maximum correlation time between the recoil implantation and ^{197}At($^1/_2^+$) α decay was set to 10 s, and 13 s between the ^{197}At($^1/_2^+$) α decay and ^{193}Bi($^1/_2^+$) α decay. The $^1/_2^+$ state in ^{193}Bi is known to have a half-life of 3.07(13) s [12], hence the chosen maximum correlation times correspond to roughly 4-5 times the half-life of each activity. As the statistics in this study are low, slightly longer correlation times were used in order to minimize losses caused by limited search times.

In Fig. 6 prompt γ-ray singles energy spectra observed in JUROGAM II with different tagging methods are shown. Panel (a) is presented for comparison, and there only recoil tagging is implemented. Most of the transitions visible in this panel belong to polonium isotopes, see Fig. 1(b). In panel (b) R-α tagging is introduced. Transitions marked with symbols may involve

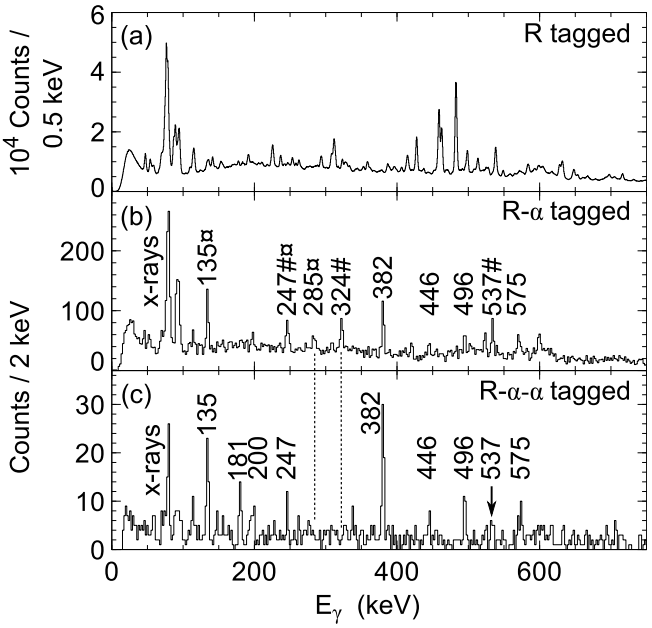

FIG. 6. Prompt γ-ray singles spectra observed in JUROGAM II array tagged by: (a) Recoil (b) Recoil - ^{197}At($^1/_2^+$) α decay (c) Recoil - ^{197}At($^1/_2^+$) α decay - ^{193}Bi($^1/_2^+$) α decay chains. Transitions marked with symbols may involve contaminant intensity from ^{198}At [28] (symbol ¤) and ^{197}At Band 2 [29] (symbol #)

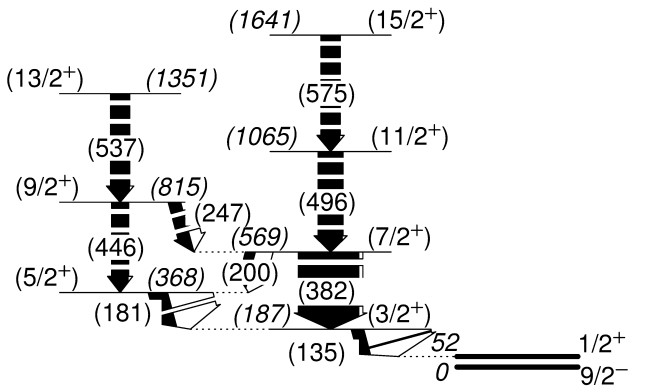

FIG. 7. Tentative level scheme for the levels feeding the $^1/_2^+$ state in ^{197}At. The intensity of the 135 keV transition is not to scale for graphical reasons. The rest of the ^{197}At level scheme is show in [29].

contaminant intensity from γ-ray transitions with overlapping transition energy from neighboring nuclei ^{198}At [28] (symbol ¤) and ^{197}At Band 2 [29] (symbol #). These contaminating transitions vanish when R-α-α tagging is implemented in panel (c).

Transitions observed using R-α-α tagging are listed in Table II. The level scheme above the $^1/_2^+$ state was constructed mainly based on the energy sum and total transition intensity information. The suggested level scheme is presented in Fig. 7. In order to extract the total transition intensities certain assumptions must be made. The 135 keV transitions is assumed to have a mixed M1/E2 character. This is a reasonable assumption because the analogous transitions in ^{199}At and ^{201}At are suggested to have a mixed M1/E2 character [5]. Statistics available for $\gamma\gamma$ coincidence analysis were rather limited. Fig. 8 shows the energy spectrum of R-α tagged γ rays, which are in coincidence with the 135-keV transition. The spectrum shows weak signs of coincident 181-, 382- and 496- keV transitions, which support the suggested level scheme.

TABLE II. Observed γ rays above the $^1/_2^+$ state in ^{197}At. I_γ is the relative γ-ray intensity and A_2 is the angular distribution parameter, both are deduced from R-α-α tagged JUROGAM II data. Internal-conversion coefficients for the calculation of total transition intensity I_{TR} were taken from [25]. I_{TR} is normalized such that the 382-keV γ-ray transition has an intensity of 100.

E_γ (keV)	I_γ	I_{TR}	A_2	I_i^π	I_f^π
135.2(6)	59(13)	370(80), 190(40)[a]	(<0)	($^3/_2^+$)	$^1/_2^+$
181.0(6)	31(8)	100(30), 54(14)[a]		($^5/_2^+$)	($^3/_2^+$)
199.9(11)[b]	16(6)	43(15)		($^7/_2^+$)	($^5/_2^+$)
246.6(7)	20(7)	38(12)		($^9/_2^+$)	($^7/_2^+$)
381.8(7)	100(20)	110(30)	(>0)	($^7/_2^+$)	($^3/_2^+$)
446.4(7)	27(9)	28(9)		($^9/_2^+$)	($^5/_2^+$)
496.4(7)	40(11)	41(12)		($^{11}/_2^+$)	($^7/_2^+$)
536.5(7)	18(7)	19(8)		($^{13}/_2^+$)	($^9/_2^+$)
575.4(7)	31(10)	32(10)		($^{15}/_2^+$)	($^{11}/_2^+$)

[a] Transition is suggested to have a mixed M1/E2 character. The two given intensity readings stand for pure M1 and E2 transition, respectively.

[b] Width of this γ peak in the spectrum refers to a possible doublet.

IV. DISCUSSION

For the first time we have observed the isomeric intruder $^1/_2^+$ state in ^{203}At. We have studied the level structure below and above this state in ^{203}At, and in addition the level structure above the $^1/_2^+$ state in ^{197}At. In ^{197}At the α-decaying state was observed for the first time already in 1986 by Coenen *et al.* [4], and later Andgren *et al.* [32] saw the first γ-ray transitions feeding the $^1/_2^+$ state.

In Fig. 9(a) the level energies of the intruder $^1/_2^+$ states in odd-Z nuclei close to lead are presented. As one may observe, the level energy for the $^1/_2^+$ state obtained in this study for ^{203}At is consistent with the systematics of the neighboring nuclei. The $^1/_2^+$ states in the neighboring nuclei are suggested to originate from a $\pi(s_{1/2})^{-1}$ configuration, see the references listed in Fig. 9 caption. In ^{199}At and heavier astatine nuclei the $^1/_2^+$ state is depopulated through an E3 type transition to the $^7/_2^-$ state. In ^{199,201}At nuclei this $^7/_2^-$ state is suggested to originate from the $\pi(f_{7/2})$ configuration [5], which is also the case in the nearby nuclei ^{203,205}Fr [7, 8]. The half-life

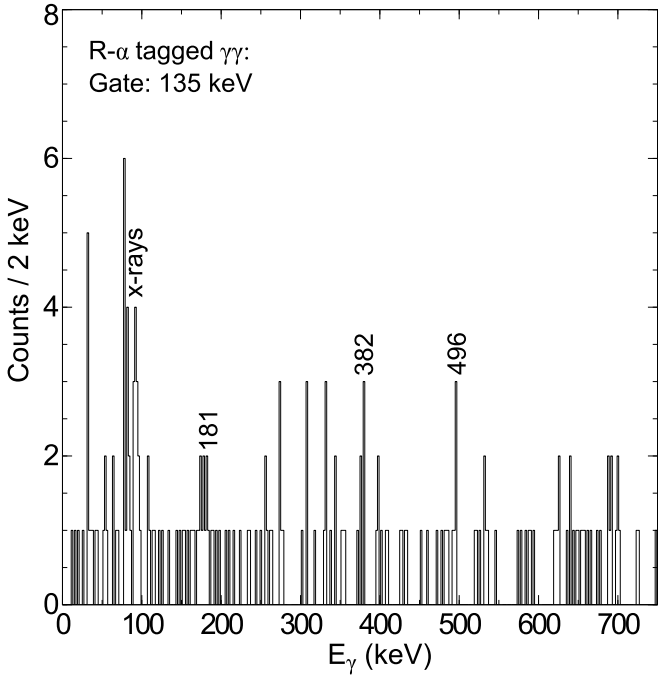

FIG. 8. Energy spectrum of R-α tagged prompt γ rays in coincidence with the 135-keV γ-ray transition.

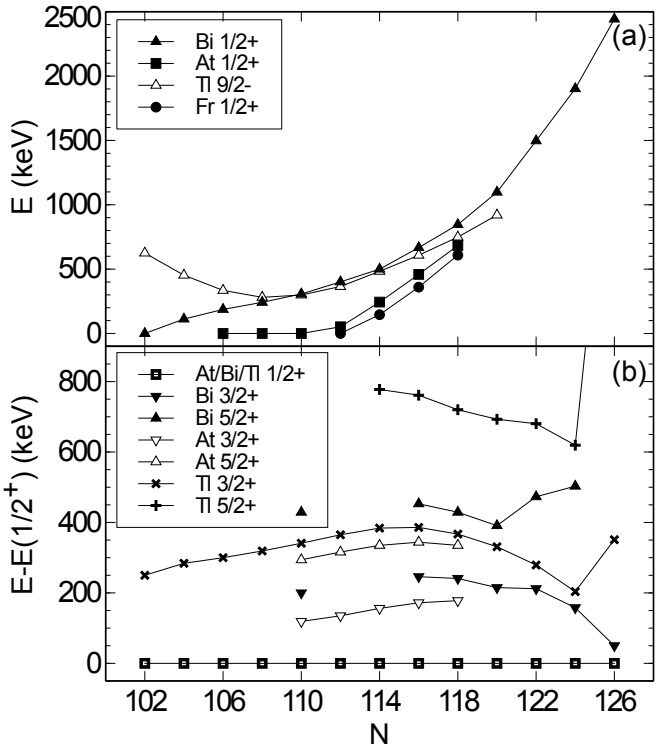

FIG. 9. Panel (a) presents the level energies of the intruder $^1/_2{}^+$ states in odd-Z nuclei above lead. These states are suggested to originate from the $\pi(s_{1/2})^{-1}$ configuration. The level energies of the $^9/_2{}^-$ state in Tl isotopes are presented for comparison. In panel (b) the level energies of the lowest $^3/_2{}^+$ ($\pi(d_{3/2})^{-1}$ in Bi and Tl nuclei) and $^5/_2{}^+$ ($\pi(d_{5/2})^{-1}$ in Bi nuclei) states are presented relative to the level energy of the $^1/_2{}^+$ state. Data for Tl isotopes were taken from [34–41], Bi [1, 2, 34, 35, 42, 43], At this work and [2, 3, 5, 32, 33] and Fr [6–8]. The neutron numbers of nuclei studied in this work are 112 and 118.

of 3.5(6) ms obtained for the $^1/_2{}^+$ state in ^{203}At corresponds to a reduced transition strength of 0.027(4) W.u. This value is comparable to values of 0.05 W.u. (^{201}At, [5]), 0.09 W.u. (^{199}At, [5]) and 0.07 W.u. (^{195}At, [33]) obtained for the analogous transitions in the neighboring At nuclei. For the reasons listed above we suggest that in ^{203}At the $^1/_2{}^+$ state originates from the $\pi(s_{1/2})^{-1}$ configuration, and the $^7/_2{}^-$ state originates from the $\pi(f_{7/2})$ configuration.

For comparison, in Fig. 9(a) the level energies of the $^9/_2{}^-$ states in thallium nuclei are also presented. These states are analogous to the $^1/_2{}^+$ states in At nuclei in a sense that in both cases a proton is excited from the $s_{1/2}$ orbital across the $Z = 82$ shell closure to the $h_{9/2}$ orbital. These $^9/_2{}^-$ states appear to follow the energies of the $^1/_2{}^+$ states in bismuth nuclei down to N=108, but in lighter thallium nuclei these states diverge.

Based on the information obtained in this study it appears to be difficult to interpret unambiguously the levels feeding the $^1/_2{}^+$ state. At least three different scenarios can be considered, none being clearly more plausible than others. These three scenarios are discussed below:

A: $\left|\pi(d_{3/2})^{-1}; {}^3/_2{}^+\right\rangle$ **and** $\left|\pi(d_{5/2})^{-1}; {}^5/_2{}^+\right\rangle$

In Fig. 9(b) the energies of the $^3/_2{}^+$ and $^5/_2{}^+$ states with respect to the level energy of the $^1/_2{}^+$ state in odd-Z thallium, bismuth and astatine nuclei are presented. The electron capture properties presented in [13] suggest that the $^3/_2{}^+$ and $^5/_2{}^+$ states in ^{203,205,207}Bi originate from the $\pi(d_{3/2})^{-1}$ and $\pi(d_{5/2})^{-1}$ configurations. In thallium the $^3/_2{}^+$ state is interpreted to originate from the same $\pi(d_{3/2})^{-1}$ configuration [34], but the $^5/_2{}^+$ state is suggested to have a mixed wave function with a $\pi(s_{1/2})^{-1} \otimes 2^+$ or $\pi(d_{3/2})^{-1} \otimes 2^+$ being the dominant component (see, for example, [44–46]).

The observed level energies for the $^3/_2{}^+$ and $^5/_2{}^+$ states in ^{197,203}At nuclei follow the corresponding levels in thallium and bismuth nuclei, and those are also consistent when compared to corresponding states in ^{199,201}At. Similarly to bismuth, the $^3/_2{}^+$ and $^5/_2{}^+$ states in ^{197,203}At can be interpreted to originate from the $\pi(d_{3/2})^{-1}$ and $\pi(d_{5/2})^{-1}$ configurations, respectively. This is also what was suggested earlier for the $^3/_2{}^+$ and $^5/_2{}^+$ states in ^{199,201}At [5].

In odd-Z nuclei above shell closures the low-lying states are often compared to the low-lying states in their lighter even-Z isotones (see, for example, [7, 8, 29, 47]). In this case the $^1/_2{}^+$ state, being a proton-hole state, can be described as a proton hole in the radon core, hence a comparison to a heavier even-Z isotone is reasonable. In Fig. 10(a) the level energies of the states above the $^3/_2{}^+$ [$^5/_2{}^+$] state are presented with respect to the level energy

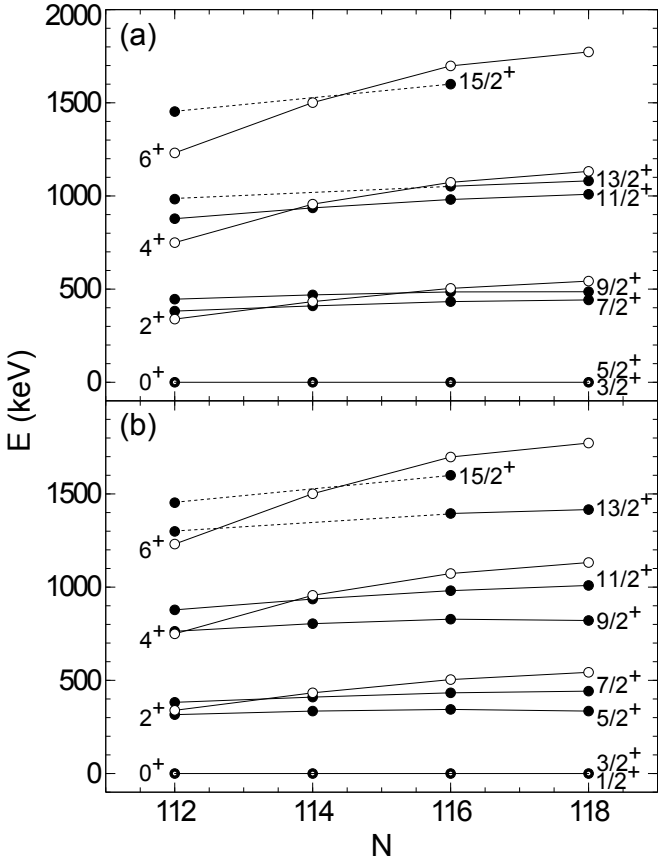

FIG. 10. In the panel (a) the level energies of the states above the $^3/_2^+$ [$^5/_2^+$] state in astatine nuclei are shown relative to the level energy of the $^3/_2^+$ [$^5/_2^+$] state. These level energies in astatine nuclei (solid symbols) are compared to the level energies of the lowest yrast states in respective radon core (open symbols). Data for At nuclei is taken from this work and [5], and for Rn nuclei from [28, 48]. Level energy of the 4^+ state in ^{200}Rn (N=114) is increased by 20 keV for visual purposes. Panel (b) is the same as panel (a), but the levels in astatine are normalized to the level energy of the $^1/_2^+$ and $^3/_2^+$ states.

of the $^3/_2^+$ [$^5/_2^+$] state. These level energies are compared to the lowest 2^+, 4^+ and 6^+ states of the respective radon isotone. The level spacing in these radon states is similar to those in astatine nuclei above the $^3/_2^+$ [$^5/_2^+$] state. Because of this similarity it can be suggested that the $^7/_2^+$, $^{11}/_2^+$, $^{15}/_2^+$ [$^9/_2^+$, $^{13}/_2^+$] states originate from the $\pi(d_{3/2})^{-1}$ $\left[\pi(d_{5/2})^{-1}\right)$] coupled to the 2^+, 4^+ and 6^+ states of the radon core. It is worth noting that some of these states in astatine nuclei have a tentative spin and parity assignments.

From Fig. 10(a) one may also notice that the excitation energies of the low-lying states in radon are pushed down as the neutron number decreases. This can be understood through the onset of deformation [28, 48]. In astatine nuclei Total Routhian surface (TRS) calculations [32] predict a sharp change in deformation between ^{195}At and ^{197}At. These calculations predict a near spherical shape for the $\pi(h_{9/2})^3$ ground state configuration in $^{197-211}$At odd-mass isotopes. The fact that the astatine states presented in Fig. 10(a) are not pushed down significantly in energy as the neutron number decreases suggests a nearly spherical shape down to ^{197}At.

The problem with this interpretation is that the spherical $\pi(d_{5/2})$ orbital is deep below Fermi surface. Therefore a hole excitation originating from it may be considered unlikely at the observed excitation energies of the $^5/_2^+$ states in astatine nuclei. The same holds if the nucleus is considered to be deformed, the $\frac{5}{2}$[402] Nilsson orbital is well separated from the $\frac{3}{2}$[402] orbital. These Nilsson states originate from the above mentioned spherical hole configurations.

B: $\left|\pi(d_{3/2})^{-1}; ^3/_2^+\right\rangle$ **and** $\left|\pi(s_{1/2})^{-1} \otimes 2^+; ^5/_2^+\right\rangle$

One may also suggest that the observed $^5/_2^+$ states in astatine nuclei originate from the $\pi(s_{1/2})^{-1}$ coupled to the 2^+ state of a respective radon core. Accordingly the $^9/_2^+$ and $^{13}/_2^+$ states above the $^5/_2^+$ state may be suggested to originate from the coupling of the $\pi(s_{1/2})^{-1}$ to the 4^+ and 6^+ states of the corresponding radon core. In this scenario the interpretation for the $^3/_2^+$ state and the states directly above it is identical to the scenario A.

Like in scenario A, also in this case a systematic comparison to the radon states can be done. This is shown in Fig. 10(b). From this comparison it is clear that there is more deviation in the level spacing between astatine and radon nuclei than what is in the systematics plot of the scenario A (Fig. 10(a)). This holds especially in the heavier isotopes of interest, but in ^{197}At the agreement is fairly good. This, however, may be merely coincidental due to down-sloping trend of the radon states.

The problem in this scenario is the absence of the $^5/_2^+ \rightarrow {}^1/_2^+$ E2 transition. This unobserved E2 transition, being collective in nature ($\left|\pi(s_{1/2})^{-1} \otimes 2^+; ^5/_2^+\right\rangle \rightarrow \left|\pi(s_{1/2})^{-1}; ^1/_2^+\right\rangle$), should be able to compete with the observed M1 transition. The M1 $\left|\pi(s_{1/2})^{-1} \otimes 2^+; ^5/_2^+\right\rangle \rightarrow \left|\pi(d_{3/2})^{-1}; ^3/_2^+\right\rangle$ transition involves a structural change, hence in the frame of scenario B it is surprising that it dominates the depopulation of the $^5/_2^+$ state.

C: $\frac{3}{2}$[402] **Nilsson state and strongly coupled rotation**

In the case of ^{197}At it can be speculated that the observed cascades above the $^3/_2^+$ state are signature partners of a rotational band build on the $\frac{3}{2}$[402] Nilsson configuration. This Nilsson state originates from the spherical $\pi(d_{3/2})^{-1}$ configuration. If this is the case then the kinematic moment of inertia $\Im^{(1)}$ can be extracted and compared to the kinematic moments of inertia of other cascades in neighboring nuclei. This is shown as a function of rotational frequency ω in Fig. 11. For clarity these data are presented in two separate panels with identical scales.

In panel (a) the kinematic moments of inertia of the cascades above $^1/_2^+$ state in astatine nuclei are presented.

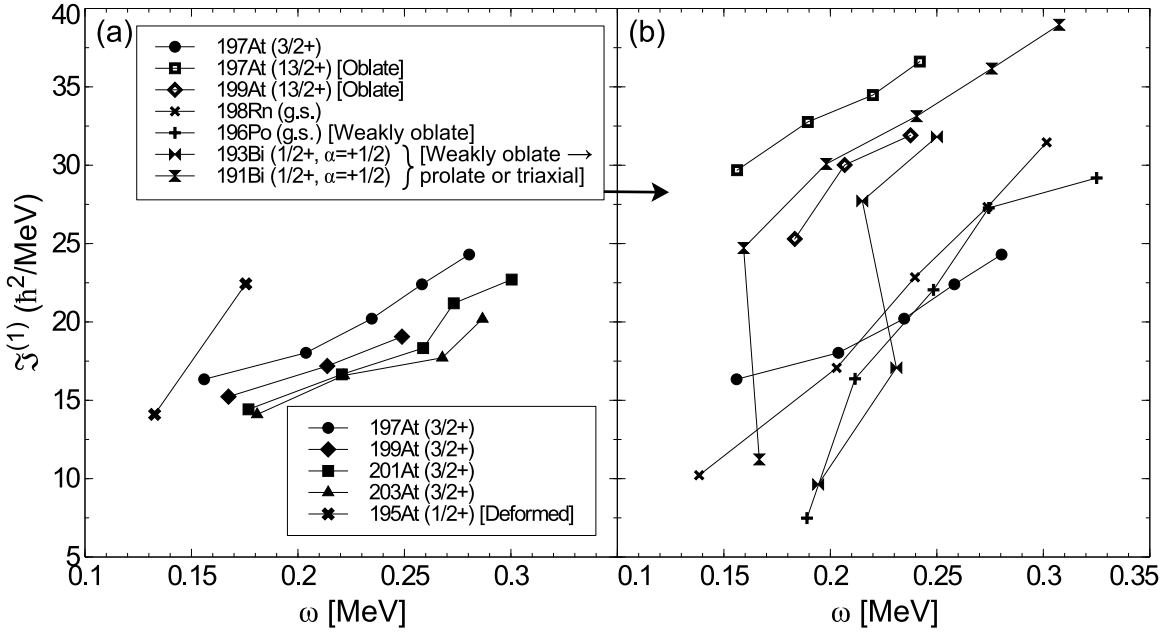

FIG. 11. Kinematic moments of inertia $\Im^{(1)}$ of selected cascades above lead as a function of rotational frequency ω. Data is presented in two panels in order to maintain the readability of the figure. See text for details.

The transition energy of the lowest transition above the $^1/_2{}^+$ states in the odd-mass $^{197-203}$At is too small to be E2 member of a rotational cascade with the transition above it. In other words, if these transitions are assumed to be the lowest E2 transitions in a rotational cascades, this would correspond to $^{E(I+4)}/_{E(I+2)}$ ratios of 3.8, 3.6, 3.5 and 3.5 for ^{197,199,201,203}At, respectively. Ratios this large are unphysical for a rotational cascade, hence the lowest transition above the $^1/_2{}^+$ state cannot be E2 member of a rotational structure in $^{197-203}$At. Because of this and the lack of the $^5/_2{}^+ \rightarrow {}^1/_2{}^+$ transition, the $^3/_2{}^+$ states are taken to be the band head state in the calculation of the kinematic moments of inertia in the odd mass $^{197-203}$At. Situation changes in ^{195}At where the $^5/_2{}^+ \rightarrow {}^1/_2{}^+$ transition is observed, and the $^1/_2{}^+$ band is suggested to be deformed [33]. From Fig. 11(a) one may notice that the kinematic moment of inertia of the ^{197}At($^3/_2{}^+$) band is comparable to the same band in heavier astatine isotopes, whereas there is a clear jump to higher kinematic moment of inertia in ^{195}At, indicating a structural change and an increase of deformation.

In Fig. 11(b) the kinematic moment of inertia of the ^{197}At($^3/_2{}^+$) band is compared to the ground state bands observed in neighboring even-even nuclei ^{196}Po and ^{198}Rn. A detailed life-time measurement [49], in-source resonant ionization laser spectroscopy [50] and a coulomb excitation [51] studies all indicate that the ground state and low lying yrast states in ^{196}Po exhibits a mixing of a spherical and weakly deformed oblate structures. From Fig. 11(b) it is clear that the kinematic moments of inertia of ^{196}Po and ^{198}Rn ground state bands and the ^{197}At($^3/_2{}^+$) band are comparable.

In the same figure the ^{197}At($^3/_2{}^+$) band is also compared to the positive signature ($\alpha = +^1/_2$) bands above the $^1/_2{}^+$ state in ^{191,193}Bi nuclei. In both bismuth nuclei it has been suggested [11, 12] that the low-spin part of these bands are weakly oblate and this low-deformation structure is crossed with a more deformed oblate or triaxial structure. This onset of deformation can be seen as an increase in the kinematic moment of inertia in Fig. 11(b). This interpretation is in agreement with a recent laser spectroscopy study of the intruder states in ^{193,195,197}Bi [52]. From the Fig. 11(b) it is clear that the kinematic moment of inertia of the ^{197}At($^3/_2{}^+$) band is less than the analogous values for the deformed parts of the ^{191,193}Bi($^1/_2{}^+$) bands, indicating a less deformed shape for the ^{197}At($^3/_2{}^+$) band. However, the kinematic moment of inertia of the ^{197}At($^3/_2{}^+$) band is slightly larger than the respective values for the weakly oblate low-spin parts of the ^{191,193}Bi($^1/_2{}^+$) bands. In Fig. 11(b) also the oblate [29] ^{197,199}At($^{13}/_2{}^+$) bands are compared to the ^{197}At($^3/_2{}^+$) band.

As discussed above, the level structure on top of the $^3/_2{}^+$ state in ^{197}At reminds a strongly coupled rotational structure, and the extracted kinematic moments of inertia appears to be comparable to the weakly oblate bands observed in nearby nuclei. Hence, one may suggest that the levels above the $^3/_2{}^+$ state in ^{197}At are a strongly coupled rotational band build on the weakly oblate $\frac{3}{2}[402]$ $\left(\pi(d_{3/2})^{-1}\right)$ configuration with possible spherical mixing, however, in the Nilsson figure the $\frac{3}{2}[402]$ orbital appears to be well separated from the $\frac{1}{2}[400]$ orbital at small oblate deformations. It is worth noting that also on the prolate side of the Nilsson scheme the $\frac{1}{2}[400]$ and $\frac{3}{2}[402]$ orbitals approach the Fermi surface. This might

also serve an explanation for the observed $^1/_2^+$ and $^3/_2^+$ states, however, there is no earlier experimental neither theoretical work that would support a prolate deformation for the nuclei of interest. It is also worth noting that the observed kinematic moments of inertia of the ^{197}At($^3/_2^+$) cascade are also comparable to the the corresponding values in heavier astatine isotopes. However, in ^{199,201,203}At the states above the $^3/_2^+$ state cannot form a strongly coupled rotational structure, because the structure on top of the $^5/_2^+$ state feeds the structure on top of the $^3/_2^+$, but not vice versa.

V. SUMMARY

We have studied the isomeric intruder $^1/_2^+$ states in ^{197,203}At. In ^{203}At the isomer and the level structure above it is observed for the first time, whereas in ^{197}At a tentative level scheme above the isomer is suggested. The isomeric state is suggested to originate from the $\pi(s_{1/2})^{-1}$ configuration in both nuclei. The observed states agree well with our earlier results and the systematics of the relevant states in this region of the chart of nuclides. However, without theoretical support it turns out to be difficult to interpret for the states feeding the isomeric $^1/_2^+$ state. None of the discussed simple interpretations fit well to the scheme of observed $^3/_2^+$ and $^5/_2^+$ states, which may of course suggest a mixed wave function for the states of interest. It remains to be seen in future experiments whether the levels feeding to the $^1/_2^+$ intruder states are spherical, oblate or even prolate. Moreover, in ^{195}At the $^1/_2^+$ state becomes the ground state, hence the scheme of observed excited states changes [33]. This makes the complete understanding of the picture even more difficult.

VI. ACKNOWLEDGMENTS

This work has been supported by the Academy of Finland under the Finnish Center of Excellence Programme (Contract number 213503). The authors also thank the GAMMAPOOL European Spectroscopy Resource for the loan of the detectors for the JUROGAM II array. Support has also been provided by the EU 7th framework programme, Project No. 262010 (ENSAR). KA acknowledges that this material is partially based upon work supported by the U.S Department of Energy, Office of Science, Office of Nuclear Physics, under contract number DE-AC02-06CH11357

[1] A. Andreyev, D. Ackermann, F. Heβberger, K. Heyde, S. Hofmann, M. Huyse, D. Karlgren, I. Kojouharov, B. Kindler, B. Lommel, G. Münzenberg, R. Page, K. Van de Vel, P. Van Duppen, W. Walters, and R. Wyss, Phys. Rev. C **69**, 054308 (2004).

[2] H. Kettunen, T. Enqvist, T. Grahn, P. Greenlees, P. Jones, R. Julin, S. Juutinen, A. Keenan, P. Kuusiniemi, M. Leino, A.-P. Leppänen, P. Nieminen, J. Pakarinen, P. Rahkila, and J. Uusitalo, Eur. Phys. A **17**, 537 (2003).

[3] H. Kettunen, T. Enqvist, M. Leino, K. Eskola, P. Greenlees, K. Helariutta, P. Jones, R. Julin, S. Juutinen, H. Kankaanpää, H. Koivisto, P. Kuusiniemi, M. Muikku, P. Nieminen, P. Rahkila, and J. Uusitalo, Eur. Phys. J. A **16**, 457 (2003).

[4] E. Coenen, K. Deneffe, M. Huyse, P. Van Duppen, and J. Wood, Z. Phys. A **324**, 485 (1986).

[5] K. Auranen, J. Uusitalo, S. Juutinen, U. Jakobsson, T. Grahn, P. T. Greenlees, K. Hauschild, A. Herzáň, R. Julin, J. Konki, M. Leino, J. Pakarinen, J. Partanen, P. Peura, P. Rahkila, P. Ruotsalainen, M. Sandzelius, J. Sarén, C. Scholey, J. Sorri, and S. Stolze, Phys. Rev. C **90**, 024310 (2014).

[6] J. Uusitalo, M. Leino, T. Enqvist, K. Eskola, T. Grahn, P. Greenlees, P. Jones, R. Julin, S. Juutinen, A. Keenan, H. Kettunen, H. Koivisto, P. Kuusiniemi, A.-P. Leppänen, P. Nieminen, J. Pakarinen, P. Rahkila, and C. Scholey, Phys. Rev. C **71**, 024306 (2005).

[7] U. Jakobsson, S. Juutinen, J. Uusitalo, M. Leino, K. Auranen, T. Enqvist, P. Greenlees, K. Hauschild, P. Jones, R. Julin, S. Ketelhut, P. Kuusiniemi, M. Nyman, P. Peura, P. Rahkila, P. Ruotsalainen, J. Sarén, C. Scholey, and J. Sorri, Phys. Rev. C **87**, 054320 (2013).

[8] U. Jakobsson, J. Uusitalo, S. Juutinen, M. Leino, T. Enqvist, P. Greenlees, K. Hauschild, P. Jones, R. Julin, S. Ketelhut, P. Kuusiniemi, M. Nyman, P. Peura, P. Rahkila, P. Ruotsalainen, J. Sarén, C. Scholey, and J. Sorri, Phys. Rev. C **85**, 014309 (2012).

[9] J. Uusitalo, J. Sarén, S. Juutinen, M. Leino, S. Eeckhaudt, T. Grahn, P. Greenlees, U. Jakobsson, P. Jones, R. Julin, S. Ketelhut, A.-P. Leppänen, M. Nyman, J. Pakarinen, P. Rahkila, C. Scholey, A. Semchenkov, J. Sorri, A. Steer, and M. Venhart, Phys. Rev. C **87**, 064304 (2013).

[10] Z. Kalaninová, A. Andreyev, S. Antalic, F. Heßberger, D. Ackermann, B. Andel, M. Drummond, S. Hofmann, M. Huyse, B. Kindler, J. Lane, V. Liberati, B. Lommel, R. Page, E. Rapisarda, K. Sandhu, i. c. v. Šáro, A. Thornthwaite, and P. Van Duppen, Phys. Rev. C **87**, 044335 (2013).

[11] Nyman, M., Juutinen, S., Cullen, D. M., Darby, I., Eeckhaudt, S., Grahn, T., Greenlees, P. T., Herzan, A., Jakobsson, U., Jones, P., Julin, R., Kettunen, H., Leino, M., Leppänen, A.-P., Nieminen, P., Pakarinen, J., Rahkila, P., Sandzelius, M., Sarn, J., Scholey, C., and Uusitalo, J., Eur. Phys. J. A **51**, 31 (2015).

[12] A. Herzáň, S. Juutinen, K. Auranen, T. Grahn, P. T. Greenlees, K. Hauschild, U. Jakobsson, P. Jones, R. Julin, S. Ketelhut, M. Leino, A. Lopez-Martens, P. Nieminen, M. Nyman, P. Peura, P. Rahkila, S. Rinta-Antila, P. Ruotsalainen, M. Sandzelius, J. Sarén, C. Scholey, J. Sorri, and J. Uusitalo, Phys. Rev. C **92**, 044310 (2015).

[13] M. Alpsten and G. Astner, Nuclear Physics A **134**, 407 (1969).

[14] M. Leino, J. Äystö, T. Enqvist, P. Heikkinen, A. Jokinen, M. Nurmia, A. Ostrowski, W. Trzaska, J. Uusitalo, K. Eskola, P. Armbruster, and V. Ninov, Nucl. Instr. Methods Phys. Res., Sect. B **99**, 653 (1995).

[15] J. Sarén, J. Uusitalo, M. Leino, and J. Sorri, Nucl. Instr. Methods Phys. Res., Sect. A **654**, 508 (2011).

[16] R. Page, A. Andreyev, D. Appelbe, P. Butler, S. Freeman, P. Greenlees, R.-D. Herzberg, D. Jenkins, G. Jones, P. Jones, D. Joss, R. Julin, H. Kettunen, M. Leino, P. Rahkila, P. Regan, J. Simpson, J. Uusitalo, S. Vincent, and R. Wadsworth, Nucl. Instrum. Methods Phys. Res., Sect. B **204**, 634 (2003).

[17] G. Duchne, F. Beck, P. Twin, G. de France, D. Curien, L. Han, C. Beausang, M. Bentley, P. Nolan, and J. Simpson, Nucl. Instrum. Methods Phys. Res., Sect. A **432**, 90 (1999).

[18] C. Beausang, S. Forbes, P. Fallon, P. Nolan, P. Twin, J. Mo, J. Lisle, M. Bentley, J. Simpson, F. Beck, D. Curien, G. deFrance, G. Duchne, and D. Popescu, Nucl. Instrum. Methods Phys. Res., Sect. A **313**, 37 (1992).

[19] C. R. Alvarez, Nucl. Phys. News **3**, 10 (1993).

[20] E. D. Mateosian and A. Sunyar, At. Data and Nucl. Data Tables **13**, 391 (1974).

[21] K. Dybdal, T. Chapuran, D. Fossan, W. Piel, D. Horn, and E. Warburton, Phys. Rev. C **28**, 1171 (1983).

[22] I. Lazarus, D. Appelbe, P. Butler, P. Coleman-Smith, J. Cresswell, S. Freeman, R. Herzberg, I. Hibbert, D. Joss, S. Letts, R. Page, V. Pucknell, P. Regan, J. Sampson, J. Simpson, J. Thornhill, and R. Wadsworth, IEEE Trans. Nucl. Sci. **48**, 567 (2001).

[23] P. Rahkila, Nucl. Instrum. Methods Phys. Res., Sect. A **595**, 637 (2008).

[24] K. Auranen and *et. al*, To be published.

[25] T. Kibédi, T. Burrows, M. Trzhaskovskaya, P. Davidson, and C. N. Jr., Nucl. Instrum. Methods Phys. Res., Sect. A **589**, 202 (2008).

[26] A. Andreyev, P. Butler, R. Page, D. Appelbe, G. Jones, D. Joss, R.-D. Herzberg, P. Regan, J. Simpson, and R. Wadsworth, Nuclear Instruments and Methods in Physics Research Section A: Accelerators, Spectrometers, Detectors and Associated Equipment **533**, 422 (2004).

[27] K. Schmidt, The European Physical Journal A **8**, 141 (2000).

[28] R. B. E. Taylor, S. J. Freeman, J. L. Durell, M. J. Leddy, S. D. Robinson, B. J. Varley, J. F. C. Cocks, K. Helariutta, P. Jones, R. Julin, S. Juutinen, H. Kankaanpää, A. Kanto, H. Kettunen, P. Kuusiniemi, M. Leino, M. Muikku, P. Rahkila, A. Savelius, and P. T. Greenlees, Phys. Rev. C **59**, 673 (1999).

[29] U. Jakobsson, J. Uusitalo, S. Juutinen, M. Leino, P. Nieminen, K. Andgren, B. Cederwall, P. Greenlees, B. Hadinia, P. Jones, R. Julin, S. Ketelhut, A. Khaplanov, M. Nyman, P. Peura, P. Rahkila, P. Ruotsalainen, M. Sandzelius, J. Sarén, C. Scholey, and J. Sorri, Phys. Rev. C **82**, 044302 (2010).

[30] M.B. Smith, R. Chapman, J.F.C. Cocks, O. Dorvaux, K. Helariutta, P.M. Jones, R. Julin, S. Juutinen, H. Kankaanpää, H. Kettunen, P. Kuusiniemi, Y. Le Coz, M. Leino, D.J. Middleton, M. Muikku, P. Nieminen, P. Rahkila, A. Savelius, and K.M. Spohr, Eur. Phys. J. A **5**, 43 (1999).

[31] J. Wauters, P. Dendooven, M. Huyse, G. Reusen, P. Van Duppen, and P. Lievens, Phys. Rev. C **47**, 1447 (1993).

[32] K. Andgren, U. Jakobsson, B. Cederwall, J. Uusitalo, T. Bäck, S. J. Freeman, P. T. Greenlees, B. Hadinia, A. Hugues, A. Johnson, P. M. Jones, D. T. Joss, S. Juutinen, R. Julin, S. Ketelhut, A. Khaplanov, M. Leino, M. Nyman, R. D. Page, P. Rahkila, M. Sandzelius, P. Sapple, J. Sarén, C. Scholey, J. Simpson, J. Sorri, J. Thomson, and R. Wyss, Phys. Rev. C **78**, 044328 (2008).

[33] M. Nyman, S. Juutinen, I. Darby, S. Eeckhaudt, T. Grahn, P. Greenlees, U. Jakobsson, P. Jones, R. Julin, S. Ketelhut, H. Kettunen, M. Leino, P. Nieminen, P. Peura, P. Rahkila, J. Sarén, C. Scholey, J. Sorri, J. Uusitalo, and T. Enqvist, Phys. Rev. C **88**, 054320 (2013).

[34] K. Heyde, P. V. Isacker, M. Waroquier, J. Wood, and R. Meyer, Phys. Rep. **102**, 291 (1983).

[35] E. Coenen, K. Deneffe, M. Huyse, P. V. Duppen, and J. L. Wood, Phys. Rev. Lett. **54**, 1783 (1985).

[36] W. Kratschmer, H. Klapdor, and E. Grosse, Nucl. Phys. A **201**, 179 (1973).

[37] F. Kondev and S. Lalkovski, Nucl. Data Sheets **112**, 707 (2011).

[38] K. H. Hicks, T. E. Ward, J. Wiggins, C. A. Fields, and F. W. N. de Boer, Phys. Rev. C **25**, 2710 (1982).

[39] D. Venos, J. Adam, J. Jursk, A. Kuklk, L. Mal, A. palek, L. Funke, and P. Kemnttz, Nuclear Physics A **280**, 125 (1977).

[40] G. Lane, G. Dracoulis, A. Byrne, P. Walker, A. Baxter, J. Sheikh, and W. Nazarewicz, Nucl. Phys. A **586**, 316 (1995).

[41] J. Batchelder, K. Toth, C. Bingham, L. Brown, L. Conticchio, C. Davids, R. Irvine, D. Seweryniak, W. Walters, J. Wauters, E. Zganjar, J. Wood, C. DeCoster, B. Decroix, and K. Heyde, Eur. Phys. J. A **5**, 49 (1999).

[42] B. Singh, Nuclear Data Sheets **108**, 79 (2007).

[43] P. Nieminen, S. Juutinen, A. N. Andreyev, J. F. C. Cocks, O. Dorvaux, K. Eskola, P. T. Greenlees, K. Hauschild, K. Helariutta, M. Huyse, P. M. Jones, R. Julin, H. Kankaanpää, H. Kettunen, P. Kuusiniemi, Y. L. Coz, M. Leino, T. Lönnroth, M. Muikku, P. Rahkila, A. Savelius, J. Uusitalo, N. Amzal, N. J. Hammond, C. Scholey, and R. Wyss, Phys. Rev. C **69**, 064326 (2004).

[44] H. Jiang, J. J. Shen, Y. M. Zhao, and A. Arima, Journal of Physics G: Nuclear and Particle Physics **38**, 045103 (2011).

[45] A. Covello and G. Sartoris, Nuclear Physics A **93**, 481 (1967).

[46] L. Rydström, J. Blomqvist, R. Liotta, and C. Pomar, Nuclear Physics A **512**, 217 (1990).

[47] K. Auranen, J. Uusitalo, S. Juutinen, U. Jakobsson, T. Grahn, P. T. Greenlees, K. Hauschild, A. Herzáň, R. Julin, J. Konki, M. Leino, J. Pakarinen, J. Partanen, P. Peura, P. Rahkila, P. Ruotsalainen, M. Sandzelius, J. Sarén, C. Scholey, J. Sorri, and S. Stolze, Phys. Rev. C **91**, 024324 (2015).

[48] D. J. Dobson, S. J. Freeman, P. T. Greenlees, A. N. Qadir, S. Juutinen, J. L. Durell, T. Enqvist, P. Jones, R. Julin, A. Keenan, H. Kettunen, P. Kuusiniemi, M. Leino, P. Nieminen, P. Rahkila, S. D. Robinson,

J. Uusitalo, and B. J. Varley, Phys. Rev. C **66**, 064321 (2002).

[49] T. Grahn, A. Dewald, P. T. Greenlees, U. Jakobsson, J. Jolie, P. Jones, R. Julin, S. Juutinen, S. Ketelhut, T. Kröll, R. Krücken, M. Leino, P. Maierbeck, B. Melon, M. Nyman, R. D. Page, P. Peura, T. Pissulla, P. Rahkila, J. Sarén, C. Scholey, J. Sorri, J. Uusitalo, M. Bender, and P. H. Heenen, Phys. Rev. C **80**, 014323 (2009).

[50] T. E. Cocolios, W. Dexters, M. D. Seliverstov, A. N. Andreyev, S. Antalic, A. E. Barzakh, B. Bastin, J. Büscher, I. G. Darby, D. V. Fedorov, V. N. Fedosseyev, K. T. Flanagan, S. Franchoo, S. Fritzsche, G. Huber, M. Huyse, M. Keupers, U. Köster, Y. Kudryavtsev, E. Mané, B. A. Marsh, P. L. Molkanov, R. D. Page, A. M. Sjoedin, I. Stefan, J. Van de Walle, P. Van Duppen, M. Venhart, S. G. Zemlyanoy, M. Bender, and P.-H. Heenen, Phys. Rev. Lett. **106**, 052503 (2011).

[51] N. Kesteloot, B. Bastin, L. P. Gaffney, K. Wrzosek-Lipska, K. Auranen, C. Bauer, M. Bender, V. Bildstein, A. Blazhev, S. Bönig, N. Bree, E. Clément, T. E. Cocolios, A. Damyanova, I. Darby, H. De Witte, D. Di Julio, J. Diriken, C. Fransen, J. E. García-Ramos, R. Gernhäuser, T. Grahn, P.-H. Heenen, H. Hess, K. Heyde, M. Huyse, J. Iwanicki, U. Jakobsson, J. Konki, T. Kröll, B. Laurent, N. Lecesne, R. Lutter, J. Pakarinen, P. Peura, E. Piselli, L. Próchniak, P. Rahkila, E. Rapisarda, P. Reiter, M. Scheck, M. Seidlitz, M. Sferrazza, B. Siebeck, M. Sjodin, H. Tornqvist, E. Traykov, J. Van De Walle, P. Van Duppen, M. Vermeulen, D. Voulot, N. Warr, F. Wenander, K. Wimmer, and M. Zielińska, Phys. Rev. C **92**, 054301 (2015).

[52] A. E. Barzakh, D. V. Fedorov, V. S. Ivanov, P. L. Molkanov, F. V. Moroz, S. Y. Orlov, V. N. Panteleev, M. D. Seliverstov, and Y. M. Volkov, Phys. Rev. C **94**, 024334 (2016).